RESEARCH PAPER

Numerical Optimization of Successive Ionic Layer Adsorption and Reaction Synthesized Zinc Oxide Thin Film as Electron Transport Layer for Organic and Perovskite Solar Cells

Sreedev Padmanabhan[1,2], Rakhesh Vamadevan[2,*], Ananthakrishnan Ajithkumar[2]

* rakheshv@am.amrita.edu

[1] Research and Development Center, Bharathiar University, Coimbatore, 641046, Tamil Nadu, India
[2] Department of Physics, Amrita School of Physical Sciences, Amrita
 Vishwa Vidyapeetham, Amritapuri, Kollam, 690525, Kerala, India

Abstract: *Organic and Perovskite solar cells have attracted much attention recently since they can be used with flexible substrates and have lower manufacturing costs. The configuration and materials employed in their construction, including the Electron Transport Layer (ETL), active layer, electrode contact, and hole transport layer greatly influence the stability and performance of these solar cells. This research focuses on the simulation of solar cells, specifically utilizing zinc oxide (ZnO) as the electron transport layer. A 0.1 molar ZnO thin film was prepared from Zinc acetate salt and was deposited on a glass substrate using the cost-effective Successive Ionic Layer Adsorption and Reaction (SILAR) method. In-depth investigations were carried out on several factors, including structural, surface, optical and numerical analysis. The obtained parameters were utilized in the General-Purpose Photovoltaic Device Model (GPVDM) software to perform numerical simulations of the organic solar cell and Perovskite solar cell. Both Organic solar cells and Perovskite solar cells were designed numerically and through careful observations, electrical parameters like Open circuit Voltage (Voc), Short circuit current (Jsc), Fill Factor (FF), and Power Conversion Efficiency (PCE) were identified. The studies indicate the promising performance of simulated solar cells with SILAR-synthesized ZnO thin film as the ETL.*

Keywords: *ZnO Thin Films, SILAR, GPVDM, Organic and Perovskite Solar Cells.*

1. INTRODUCTION

Thin film solar cells have gathered much attraction over the two decades owing to their peculiar properties like flexibility, miniaturized design, the possibility of large-area deposition, availability of different deposition methods etc, at low cost [1-3]. The thin film layer in solar cells, which absorbs the light photons and generates the carriers are called active material. Two main types of thin film Solar cells are Organic and Perovskite solar cells based on the selection of active materials [4-7]. Organic materials like P3HT: PCBM blend is a common active material in Organic solar cells [8-10], whereas material like $CH_3NH_3PbI_3$ is commonly used as active material in Perovskite solar cells [11-13]. Organic solar cells have the main advantage of a non-toxic nature [14-15] over Perovskite solar cells but the performance and efficiency of Perovskite solar are largely preferred over organic solar cells [16-17]. The introduction of different materials and extensive research resulted in the leap in efficiency of Perovskite solar cells from 3%-25% over the last decade [18-20].

The electron transport layer (ETL) is an n-type thin film layer used for the transportation of extracted electrons to the cathode and to block the transportation of holes [21-22]. Due to *ZnO's* remarkable characteristics, *ZnO* is widely used as an electron transport layer (ETL) in Organic and Perovskite solar cells [23-25]. Properties like transparency, good optoelectronic conductivity, wide optical band gap, low exciton binding energy of 60 meV, non-toxicity, and ease of deposition methods, make zinc oxide (*ZnO*) highly suitable as an n-type semiconductor material in thin film solar cells. *ZnO* thin films also exhibit a range of other unique physical properties, such as high chemical stability, low dielectric constants, strong photoluminescence, and excellent piezoelectric properties [26-30]. Due to these remarkable characteristics of the *ZnO* thin films, extensive research has been ongoing in this field in recent years [31-33]. Successive ionic layer adsorption and reaction (SILAR), a versatile and cost-effective technique, has been proven effective for depositing ZnO thin films at room temperature [34-36]. By adjusting the deposition environment, the properties of the

thin film can be precisely controlled in SILAR, which can result in thin films with good adhesion on the substrate. The method produces homogenous and uniform films, which makes it ideal for applications that require consistent properties over large areas. Overall, SILAR is a promising approach for the development of thin films in fields such as electronics, optics, and sensors.

General Purpose Photovoltaic Device Model (GPVDM) is powerful modelling software that enables the simulation of the optical parameters of various layers in a solar cell or optoelectronic device [37-39]. With GPVDM, it is possible to investigate the effects of series and shunt resistances and analyze the device's J-V curves. The GPVDM accurately simulates transport, carrier trapping, and de-trapping using a finite drift-diffusion model. This enables the software to carry out detailed electrical simulations, which can be used to optimize the performance of photovoltaic devices and improve their efficiency. GPVDM is a valuable tool for researchers and engineers working in the field of solar energy, as it allows for the thorough analysis and characterization of different materials and device architectures. The fill factor, calculated as the difference between the device's theoretical maximum power (P_{max}) and the maximum power point (P_{mpp}), is provided by the j-v curve.
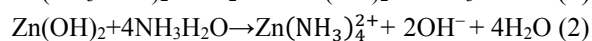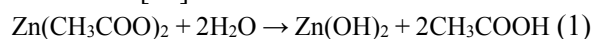
GPVDM was utilized to study the performance of organic and perovskite solar cells by researchers in which solar cell performance was identified to be depending on layer thicknesses. Dita Puspita et.al studied organic P3HT: PCBM solar cells using GPVDM, by varying the different layer thicknesses, and optimized power conversion efficiency by reporting an increase in efficiency of the organic cell from 4.16% to 4.81% [40]. Amit Kumar Mishra et.al used a GPVDM simulator for the analysis of $CH_3NH_3PBI_3$ perovskite solar cell and identified that, by changing the active layer thickness to 2×10^{-7} m, a maximum efficiency of 5.6% is obtainable for the designed perovskite solar cell [41]. According to the current National Renewable Energy Laboratory (NREL) solar cell efficiency chart, the maximum efficiency reported for organic, and perovskite solar cells are 19.2% and 26.1% respectively. The current work is unique because it thoroughly examines the use of experimentally observed zinc oxide (ZnO) thin film parameters

for simulating the electron transport layer (ETL) in perovskite and organic solar cells. The affordable Successive Ionic Layer Adsorption and Reaction (SILAR) method is used, which provided ETL for simulation and enhanced efficiency of the solar cells compared to literature values. By carefully analyzing and identifying crucial electrical characteristics including, Open circuit Voltage (Voc), Short circuit current (Jsc), Fill Factor (FF), and Power Conversion Efficiency (PCE), this work opens the door for advancements in the design and optimization of adaptable, reasonably priced solar energy harvesting systems. It also offers useful details regarding the promising performance of solar cells that use ZnO thin films that SILAR synthesizes as ETLs. This work provides a means of verifying the effectiveness of thin-film samples that have been experimentally prepared as solar cell layers before layer-by-layer deposition of solar cells.
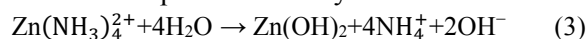
2. EXPERIMENTAL PROCEDURES

2.1. Preparation of ZnO Thin Films by SILAR Method

A 0.1 molar ZnO precursor solution was prepared by adding Zinc acetate [$ZnC_4H_6O_4$] to 100 ml of distilled water, which was subsequently stirred with a magnetic stirrer operating at 800 rpm. The formation of hydroxides in the precursor solution was prevented by adding an appropriate amount of ammonium blend solution. The presence of ZnO formation is indicated by the transformation of the solution into a transparent solution with a pH of 9. The formation of ZnO thin film from Zinc acetate salt in the SILAR method could be as follows [42].

$$Zn(CH_3COO)_2 + 2H_2O \rightarrow Zn(OH)_2 + 2CH_3COOH \ (1)$$
$$Zn(OH)_2 + 4NH_3H_2O \rightarrow Zn(NH_3)_4^{2+} + 2OH^- + 4H_2O \ (2)$$
Zinc tetra amine ion $Zn(NH_3)_4^{2+}$ breaks down in hot water to produce zinc hydroxide.
$$Zn(NH_3)_4^{2+} + 4H_2O \rightarrow Zn(OH)_2 + 4NH_4^+ + 2OH^- \quad (3)$$
$$Zn(OH)_2 \rightarrow ZnO + H_2O \quad (4)$$
SILAR deposition was conducted for deposition cycles of 15 dips, and the anionic distilled water was maintained at 80 degrees Celsius. The resulting thin film of ZnO was subsequently annealed at a temperature of 450°C for one hour.

2.2. Characterizations

The obtained sample was subjected to optical

analysis using a UV-visible spectrometer (JASCO-V-550). X-ray diffraction (XRD-BRUKER AXS D8 ADVANCE), Scanning electron microscopy (SEM-JSM-JEOL 6390) and Atomic force microscopy (AFM- VEECO Di-3100), methods were used to analyze the surface characteristics, structural characteristics and chemical quality of the resulting sample.

3. RESULTS AND DISCUSSION

3.1. Structural Analysis of ZnO Thin Film Sample

XRD spectra of the ZnO thin film is shown in Fig. 1. The samples showed crystalline nature with three distinct peaks corresponding to (1 0 0), (0 0 2), and (1 0 1) planes. The diffraction peaks at 2θ angles 31.70°, 34.38°, and 36.18° reveal the hexagonal wurtzite structure of the deposited ZnO samples (JCPDS data card no: 79-2205). The corresponding JCPDS data values are 31.79°, 34.41° and 36.25° respectively. [43-44]. The maximum intense peak was identified for the (1 0 0) plane, indicating the deviation of its growth from the direction normal to the substrate. The peak intensities are comparable in all planes, indicating the probability of clustered growth with polycrystalline nature [45-46]. Figure 1 also gives us an idea about the purity of the sample by providing only characteristic peaks corresponding to ZnO. The sample was exposed to X-rays having an approximate wavelength of 1.54° A, generating the X-ray diffraction pattern, specifically, $cu-k\alpha$ radiation [47].

$$n\lambda = 2dsin(\theta) \tag{5}$$

Bragg's equations can be used to calculate the distance (d), also known as the d-spacing, between (hkl) planes in a crystal. These equations utilize the angle of incidence (θ)at which X-rays interact with the planes, the X-ray wavelength (λ), and an integer(n) to determine the d-spacing [47].

$$D = \frac{0.9\,\lambda}{\beta\,cos\,\theta} \tag{6}$$

The Scherer formula helps to calculate the crystallite size (D) by using parameters such as

the X-ray wavelength (λ), the full width at half-maximum (FWHM) of the X-ray diffraction peak (β) in radians, and the Bragg's diffraction angle (θ). Additionally, the atomic packing factor can be determined by evaluating the ratio of lattice parameters c/a, while the volume of the cell is identified as [47]

$$V = 0.866a^2c \tag{7}$$

The equation determines the positional parameter [47].

$$u = \frac{a^2}{3c^2} \tag{8}$$

with which the bond length L is identified as [47]

$$L = \sqrt{\left(\frac{a}{3}\right)^2 + \left(\frac{1}{z} - u\right)^2 c^2} \tag{9}$$

Dislocation density and strain of the sample could be identified respectively with the equations [47].

$$\text{Dislocation density} = \frac{1}{D^2} \tag{10}$$

and

$$\text{Strain} = \frac{FWHM}{4\,tan\,(\theta)} \tag{11}$$

The XRD analysis indicates the ZnO thin film sample is available with comparable values of lattice parameters, and atomic packing fraction as available in literature for ZnO [48-49]. The sample obtained was observed to have less value of dislocation and strain. The calculated parameters are shown in Table 1.
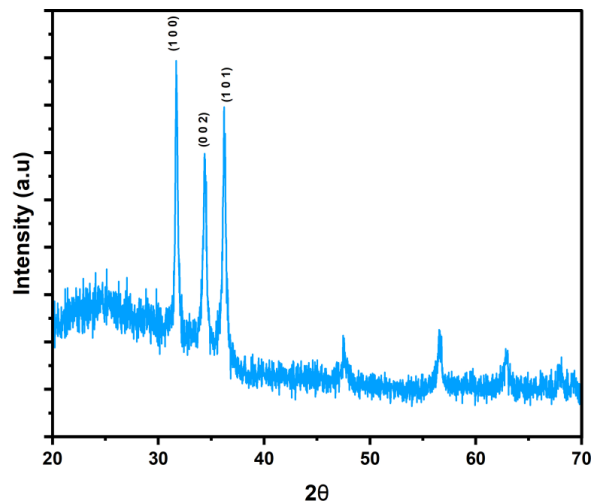

Fig. 1. XRD spectra of ZnO thin film sample

Table 1. Lattice parameters, atomic packing factor, cell volume, positional parameter, bond length, dislocation density and strain of the ZnO thin film sample

Lattice parameters (A⁰)		Crysttalite size (d) (nm)	Atomic packing factor (c/a)	Volume V (A⁰)³	Positional parameter u	Bond length L(Zn-O) (A⁰)	Dislocation density δ×10⁻³(A⁰)⁻²×10⁻⁵	Strain ɛ (rad)
a	c							
3.242	5.193	34.41	1.603	47.736	0.379	1.979	0.8445	0.007

3.2. Morphological Analysis of ZnO Thin Film Sample

SEM analysis

The surface morphology of the obtained thin film sample of ZnO, is depicted in Fig. 2. Non-uniform crystallized growth was identified for the sample. Agglomerated grains with variable crystallite sizes were visible and were non-uniformly distributed over the surface of the substrate. Agglomeration leads to the crystallized growth of microscale stone-like particles on the film surface. These formations may be due to different conditions like the chemical's pH, the medium's charge distribution, etc [46]. This non-uniformity over the surface can cause a reduction in optical transmission and electrical conductivity.
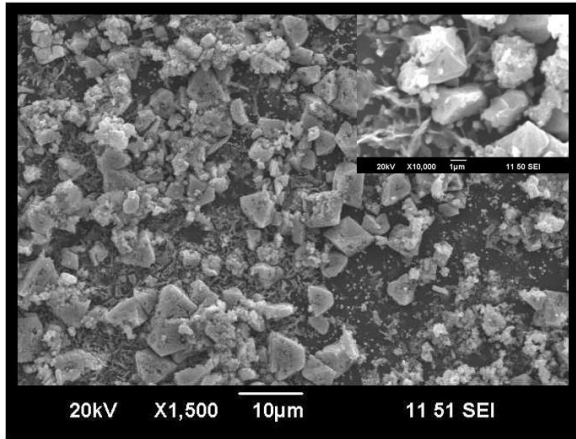

Fig. 2. SEM image of ZnO thin film sample

3.3. AFM analysis

Fig. 3 represents a 4µ m ×4 µm AFM image in 2D and 3D of the prepared sample. AFM analysis allows for the determination of specific roughness values such as root mean square roughness (R_q), average roughness (R_a), ten-point average roughness (R_z), and the line's roughness kurtosis (R_{ku}) [50-52].

$$R_q = \sqrt{\frac{z_1^2 + Z_2^z + \dots + Z_N^2}{N}} \qquad (12)$$

The surface is analyzed to estimate the roughness parameters by considering the deviation in height (z_i) of each measured point from the mean plane height, with N representing the total number of points measured.

$$R_a = \frac{1}{n}\sum_{i=1}^{n}|z_i| \qquad (13)$$

'Ra' represents the arithmetical mean deviation of the surface profile, where it quantifies the average amplitude deviation of the workpiece specimen surface at i^{th} waviness profile departure (z_i) for the number of waviness profile departures (n).

$$R_{ku} = \frac{1}{NRq^4}\left(\sum_{i=1}^{N} Y_i^4\right) \qquad (14)$$

Y is the profile's height at point i

$$Rz = \frac{1}{n}\left(\sum_{i=1}^{n} P_i - \sum_{i=1}^{n} V_i\right) \qquad (15)$$

'n' represents the number of sampling points along the assessment length. 'Pi' corresponds to the height of the ith peak, while Vi represents the depth of the ith valley, describing the characteristics of the line profile. The height distribution profile of the synthesized sample is shown in Fig. 4.
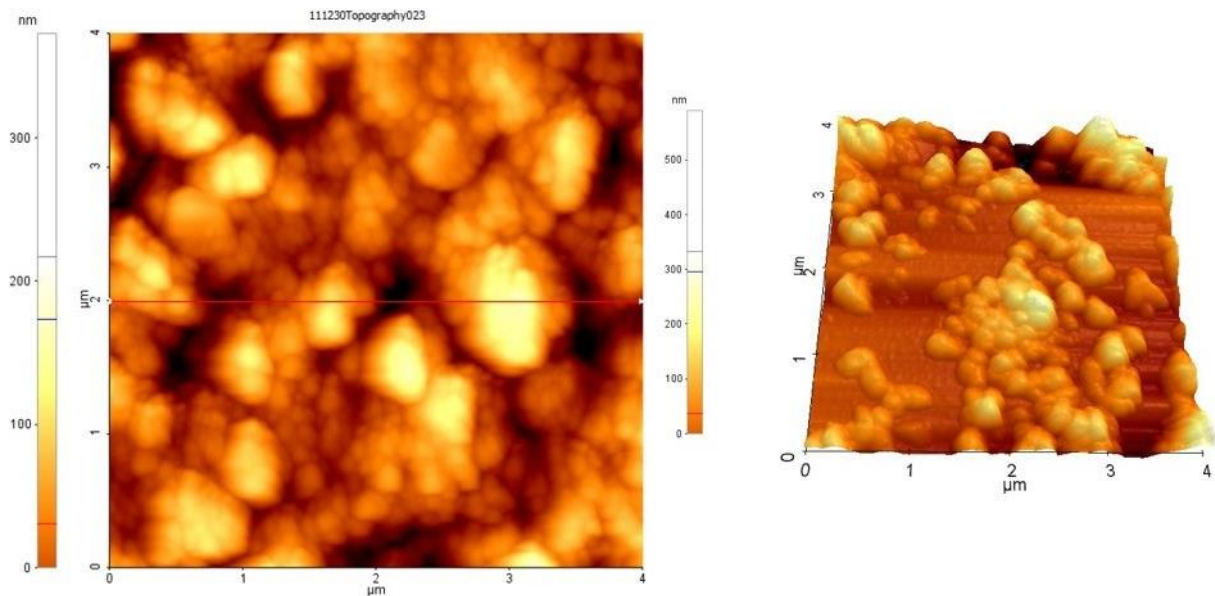

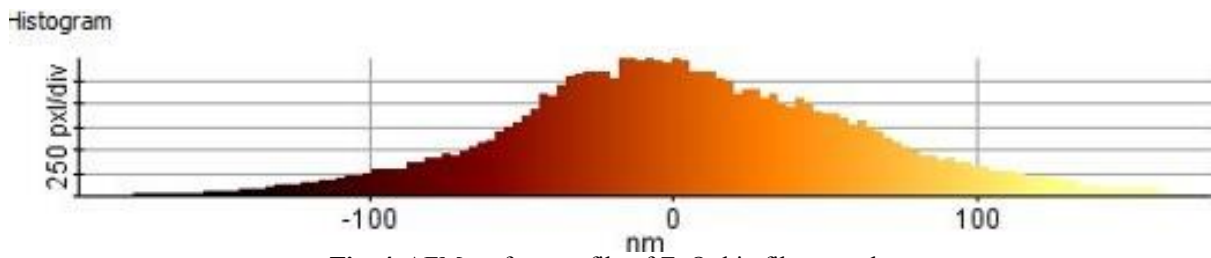**Fig. 3.** 2D and 3D AFM images of ZnO thin film sample

4

Fig. 4. AFM surface profile of ZnO thin film sample

ZnO thin films produced using zinc acetate reveal the presence of larger grains. ZnO film roughness parameter values Rq, Ra, Rz, and Rku are measured by AFM analysis and the obtained values are mentioned in Table 2. Significantly, the ratio of the Rq to the Ra is 1.204, which offers valuable insights for selecting the sample in engineering applications.

3.4. Optical Analysis of ZnO Thin Film

3.4.1. UV-Visible Spectroscopy

Fig. 5 and Fig. 6 represent the Wavelength versus Transmittance and wave-length versus Absorption coefficient of the performed ZnO sample. Transmittance, a dimensionless intensity ratio, is crucial in understanding the behavior of light passing through a material. From 200 nm to 300 nm, the transmittance value [T%] is meager; however, beyond 300 nm, there is a notable increase in transmittance, signifying a greater passage of light through the material.
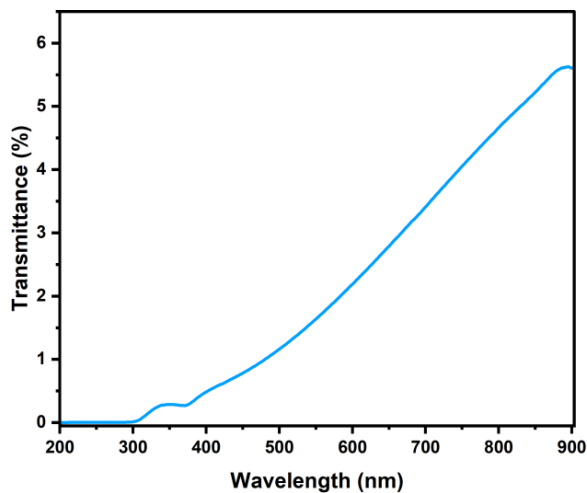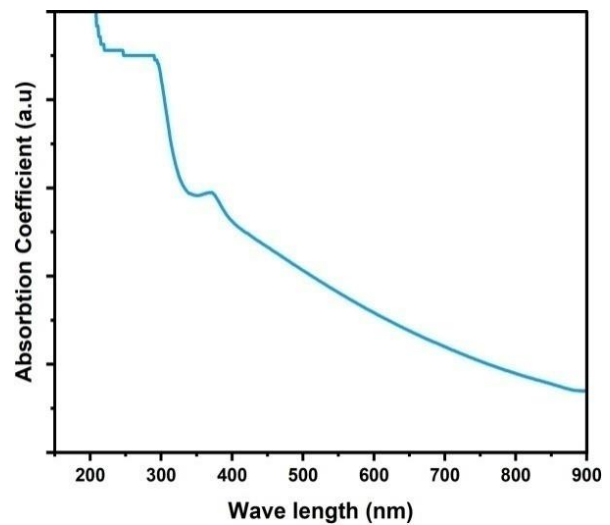

Fig. 6. Wavelength vs Absorbance Coefficient thin film sample

The transmission variation peaks at higher percentage values for higher wavelength ranges. Here a significant relation between wavelength and transmittance is exhibited by the prepared sample within the wavelength of range 300 nm to 800 nm. This specific transmittance detail illustrates the material's ability to transmit a range of visible incident light through it. As the wavelength varies from 200 nm to 900 nm, the absorption coefficient exhibits a decreasing pattern. This suggests that the material becomes less absorbent to incident light as the wavelength increases, resulting in a higher transmittance [53]. Overall, these findings highlight the material's unique characteristics in terms of transmittance, wavelength-dependency, and absorption coefficient, offering valuable insights into various fields such as optics and photovoltaics.

Fig. 5. Wavelength vs Transmittance of ZnO thin film sample

Table 2. R_q, R_a, R_z and R_{ku} values of samples

R_q(nm)	R_a(nm)	R_z (nm)	R_{ku} (nm)
110.093	91.437	294.381	2.431

Fig. 7 depicts the variation between wavelength versus extinction coefficient of the ZnO sample respectively. The relationship between the extinction coefficient and wavelength can reveal valuable insights into the optical properties and behavior of the ZnO sample. By analyzing the plot, we can observe the variation in the intensity of light absorption or scattering as a function of wavelength. Different materials exhibit unique extinction coefficient profiles, which can be influenced by factors such as composition, atomic structure, and electrical properties. The extinction coefficient versus wavelength plot helps to identify key absorption peaks or regions where the ZnO sample exhibits enhanced light absorption or scattering. These features can be indicative of specific optical properties, such as band gaps or resonant frequencies [54], which are relevant for various applications in optoelectronics and photonic devices. The extinction coefficient, denoted by k, quantifies the damping of an electromagnetic wave as it propagates through the medium. The plot of extinction coefficient (k) against wavelength provides important information about the interaction between light and the ZnO sample. The extinction coefficient represents the damping or attenuation of an electromagnetic wave as it traverses through the medium. The extinction coefficient here describes how the ZnO material absorbs and scatters light at various wavelengths.

$$\kappa = \frac{\lambda a}{4\pi} \qquad (16)\ [53]$$

Here, λ denotes wavelength, while α denotes the absorption coefficient. The peak with the highest intensity is observed at a wavelength of 290 nm, corresponding to an extinction coefficient value of 7×108. Fig. 8 depicts the variation between wavelength versus refractive index of the ZnO sample respectively. By examining the relationship between wavelength and refractive index, we can gain an understanding of how ZnO interacts with light of different wavelengths. The refractive index profile can reveal important optical phenomena, such as the dispersion of light and the material's response to different wavelengths [55]. The refractive index of a material decides the velocity with which the light will be able to traverse through it and it has no unit. From the plot, the refractive index of the sample decreases until the wavelength of 500 nm. After that wavelength, there is no change in the

refractive index by increasing the wavelength [56]. The wavelength versus refractive index plot serves as a valuable tool for understanding the optical behavior of the ZnO sample, enabling researchers to explore its dispersion properties and potential applications in various optical systems.
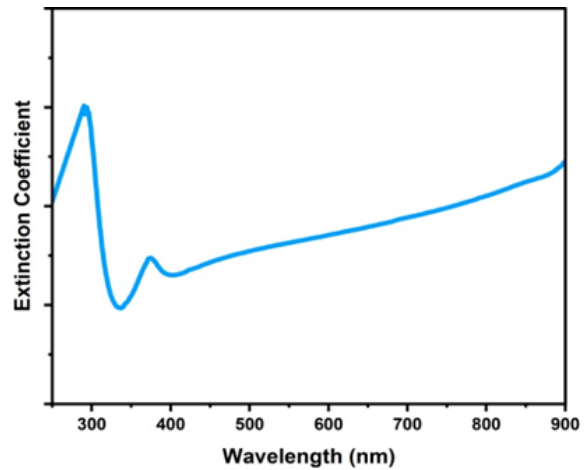

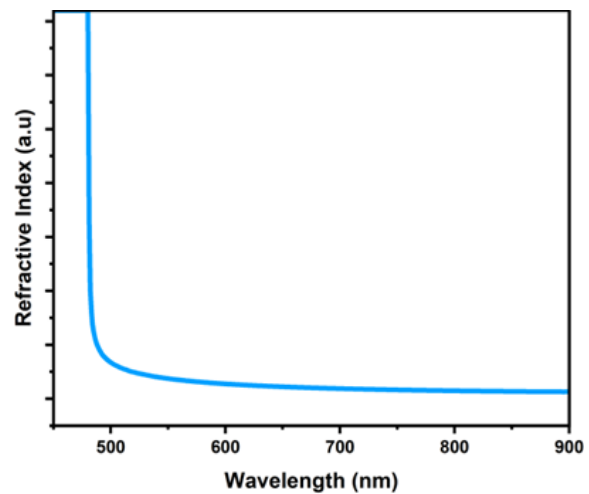**Fig. 7.** Wavelength v/s extinction coefficient of ZnO thin film sample

Fig. 8. Wavelength v/s Refractive Index of ZnO thin film sample

Fig. 9 and Fig. 10 show the relation between photon energy Vs $\alpha h\nu^2$ and $\ln\alpha$ vs $h\nu$ respectively. The linear absorption coefficient is represented by α, the Planck constant by h, and the frequency of light by ν in this context. By analyzing the plot, we can determine the optical energy gap (E_g) of the sample by extrapolating a line from the tangent of the plot and observing the point of intersection with the x-axis. This inter-accepted x-axis value corresponds to the E_g value. Based

on our observations, we will be able to identify the optical band gap energy (E_g) as 3.625 eV. The comparatively high value of E_g obtained could be considered due to the compressive stress, which will offer a wider band gap due to the increased repulsion happening between Oxygen 2p and Zinc 4s bands [57]. This strain may be generated in the lattice either due to the chemical properties of the precursor medium or due to the mismatching happening between film and substrate due to their difference in thermal coefficients [58].
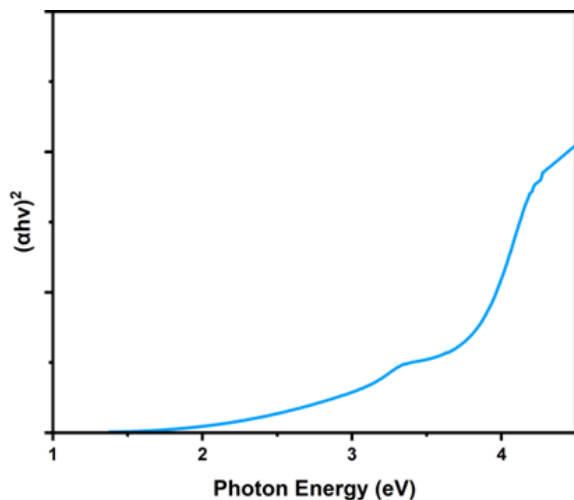

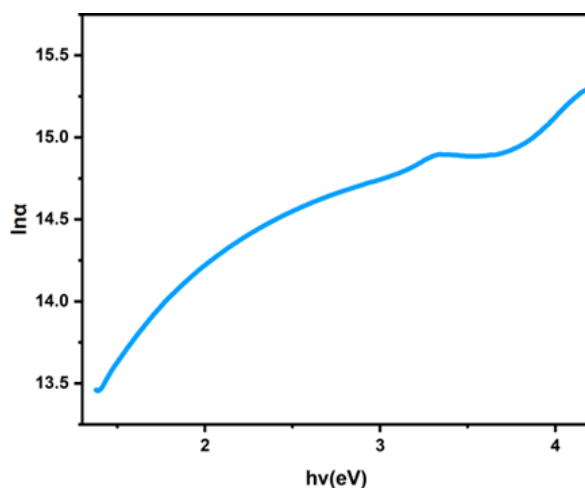**Fig. 9.** Photon Energy vs (αhv)^2 of ZnO thin film sample

Fig. 10. Urbach Energy of ZnO thin film sample

The plot of *lnα* versus *hv* offers valuable insights into the sample's Urbach energy (E_u). The Urbach energy tail provides the measure of disorder relating to the width of localized states [59]. It is possible to express the Urbach energy tail towards

the band edges in terms of the absorption coefficient's (α) spectrum dependency. The slope of the plot is calculated as the ratio of the y-axis *lnα* to the x-axis *hv*. To determine the Urbach energy, we take the inverse of the slope, resulting in a value of 1075.75 meV. The higher value obtained for E_u for the synthesized ZnO thin film sample emphasizes the defects that may have developed during the deposition. The notably higher Urbach energy (E_u) value observed in the synthesized ZnO thin film sample shows the existence of significant defects, likely originating from the deposition process [60].

3.5. Thin Film Solar Cell Parameters

It is crucial to investigate the key factors influencing the performance to increase the organic solar cell's capacity for power conversion. In this study, the GPVDM program was carried out to simulate the behavior of an OSC. Specifically for polymer-based combinations such as P3HT and PCBM, this model incorporates both electrical and optical characteristics. While the active layer of the OSC is the primary focus of the electrical simulation, the j-v curve effectively demonstrates the relationship between current density (J_{sc}) and voltage (V_{oc}). Furthermore, V_{oc} is defined as the energy difference between the (LUMO) lowest unoccupied molecular orbital and the (HOMO) highest occupied molecular orbital (HOMO), where HOMO is the donor level and LUMO is the acceptor level. The j-v curve provides the fill factor, the difference between the device's theoretical maximum power (P_{max}) and the maximum power point (P_{mpp}).

The percentage of the fill factor can be found as [61-62]

$$FF = \frac{V_{max} \times I_{max}}{V_{oc} \times I_{sc}} \quad (17)$$

The power obtained at the maximum level in comparison to the total values of the open circuit voltage and short circuit current is measured by the Fill Factor (FF). The solar cell's ability to convert energy into the electrical current is measured by the ratio of its power output (P_{out}) to its power input (P_{in}), which may be computed as [62],

$$\eta = \frac{V_{oc} \times J_{sc} \times FF}{P_{in}} \quad (18)$$

3.6. Simulation of Organic Solar Cell Using GPVDM

The P3HT: PCBM polymer solar cell, which uses a combination of Poly(3- hexylthiophene) (P3HT) and 6,6-phenyl-C_{16}-butyric acid methyl ester (PCBM) as the active layer, is one of the most popular organic solar cell structures. The donor's highest occupied molecular orbital and the acceptor's lowest unoccupied molecular orbital levels of a solar cell determine its optimal operation. While PCBM is a fullerene derivative and an n-type acceptor, P3HT is a polymer semiconductor meeting the p-type donor requirement. P3HT monomer is produced when a hexyl group is added to the thiophene ring. PEDOT:PSS, or poly(3,4-ethylenedioxythiophene): poly(styrene sulfonic acid), is a highly significant and effective conducting polymer layer that acts as the hole transport layer (HTL) in thin film solar cells, which allows the hole transportation through it but blocks the electrons [63]. Outstanding qualities of PEDOT: PSS include its great transparency in the visible spectrum, outstanding film-forming abilities, remarkable thermal stability, and most significantly, its capacity to achieve increased and tunable conductivity via doping [64]. ITO and Ag are selected respectively as hole and electron-collecting electrodes [65]. The required data for simulation of the PEDOT: PSS layer and ITO is obtained from the literature [66-67]. The simulated Organic solar cell with the experimentally obtained ZnO ETL and optimized values of Active layer and HTL is presented in Fig. 11.

The density of states (DoS) values of the P3HT:

PCBM active layer, which was utilized for GPVDM simulation available in the database, are provided in Table 3 [68].
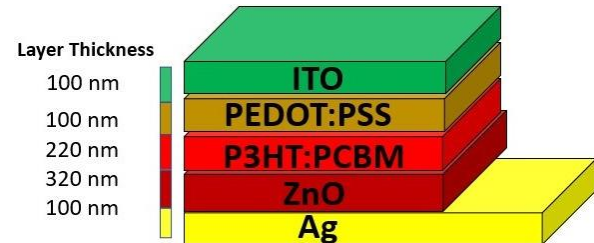

Fig. 11. Simulated Organic Solar cell with layer Thickness

Fig. 12 represents the Normalized Photons Absorbed in the simulated solar cell. Normalized photon absorbed refers to the calculation or analysis of the quantity of absorbed incident light by a solar cell or by a photovoltaic device, taking into account the wavelength-dependent absorption characteristics of the material. The normalized photons absorbed data can provide information regarding the efficiency of the solar cell and help in optimizing its design. The short circuit current of a solar cell is proportional to the number of photons absorbed. Hence the comparative analysis of active material's normalized photon absorption profile can reveal the efficiency of solar cells [69]. By studying the absorption profile, we can identify regions where light absorption is low and explore strategies to improve it, such as adjusting layer thicknesses, materials, or surface textures.

Table 3. Device parameters: The density of states (DOS) parameters utilized for the organic solar cell simulation

|			
Electron trap density	N_e^{exp}	3.8×10^{26}	$m^{-3} eV^{-1}$
Hole trap Density	N_h^{exp}	1.45×10^{25}	$m^{-3} eV^{-1}$
Electron tail slope	N_e^U	40×10^{-3}	eV
Hole tail slope	N_h^U	60×10^{-3}	eV
Number of traps		20	
Free electron to trapped electron		2.5×10^{-20}	m^{-2}
Free hole to trapped hole		4.86×10^{-22}	m^{-2}
Trapped electron to free hole		1.32×10^{-22}	m^{-2}
Trapped hole to free electron		4.67×10^{-26}	m^{-2}
Recombination rate constant	n_{free} to p_{free}	0	$m^3 s^{-1}$
Electron mobility	μ_{n0}	2.48×10^{-7}	$m^2 V^{-1} s^{-1}$
Hole mobility	μ_{p0}	2.48×10^{-7}	$m^2 V^{-1} s^{-1}$
Relative permittivitty	ε_r	3.8	au
Effective density of free electron states	N_c	1.28×10^{27}	m^{-3}
Effective density of free hole states	N_v	2.86×10^{25}	m^{-3}
Affinity	χ_i	3.8	eV
Band gap energy	E_g	1.1	eV
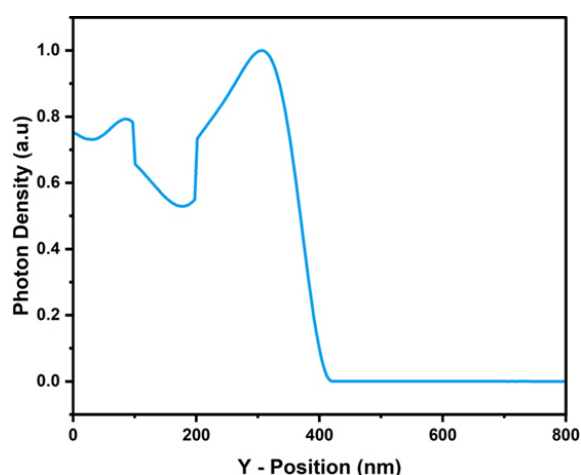
Fig. 12. Normalized Photons Absorbed in the organic solar cell

In Fig. 13, the Photon distribution absorption plot depicts the behavior of a simulated solar cell, highlighting the conditions that yield maximum fill factor (FF), open-circuit voltage (V_{oc}), power conversion efficiency (PCE), and short-circuit current density (J_{sc}) values. It can be observed that when the energy of the charge carriers surpasses the band gap of the active layer, there is a higher probability of generating and effectively collecting charge carriers within the active layer of the solar cell. It results in; the appreciable fill factor value, indicating enhanced charge carrier collection and improved device performance [70]. Fig. 14 represents the J-V curve of the simulated organic solar cell. It typically refers to the current-voltage (IV) characteristic of a solar cell or photovoltaic device. The curve provides information about the electrical behavior of the device under different operating conditions. The J-V curve offers valuable insights into the device's behavior, such as its open-circuit voltage (V_{oc}), short-circuit current (I_{sc}), maximum power point (MPP), and overall efficiency. By studying the J-V curve, we can optimize the device design and operating conditions to achieve the desired performance. The fabricated solar cell yielded a short-circuit current density (J_{sc}) of -117.35 A/m^2 and an open-circuit voltage (V_{oc}) of 0.604 V. The fabricated solar cell demonstrated remarkable performance with an FF of 0.672 and a PCE of 4.765%. These results highlight the significant potential of the cell for efficient energy conversion in photovoltaic applications. The values obtained from the analysis are shown in Table 4.

3.7. Study of Simulated Organic Solar Cell Performance by Varying the ETL Thickness

To investigate the impact of ZnO as an electron transport layer in an organic solar cell, a simulated device configuration of ITO/PEDOT: PSS/P3HT: PCBM/ZnO/Ag was utilized. The study aimed to explore the properties of the ZnO layer, particularly as an electron transport medium, by examining the effects of varying its thickness. In the simulation process, the optical properties of the ZnO layer were incorporated using experimentally derived optical parameters. Initially, the simulation focused on determining the ideal thickness of the active material to maximize the generation of charge carriers.
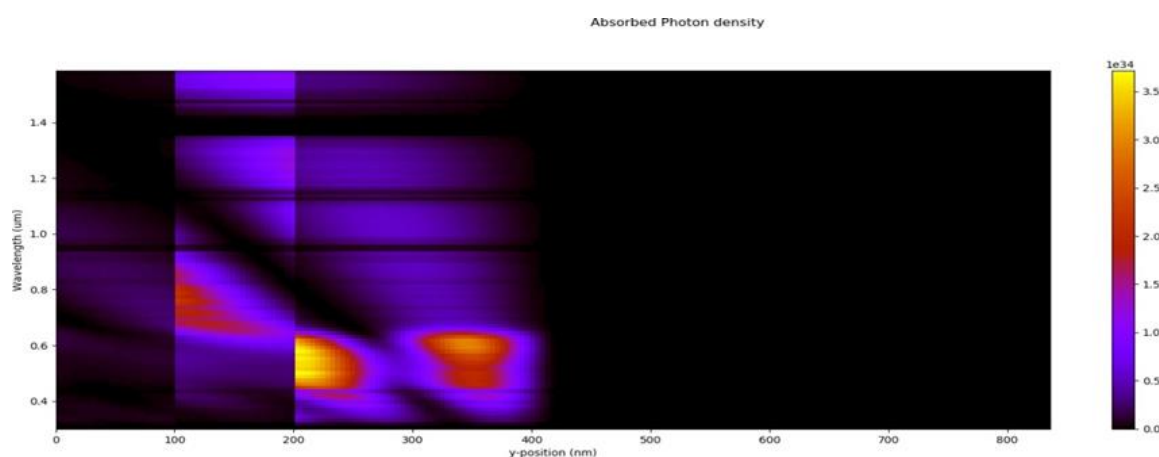

Fig. 13. Absorbed photon density in the organic solar cell

Table 4. Organic Solar cell output parameters

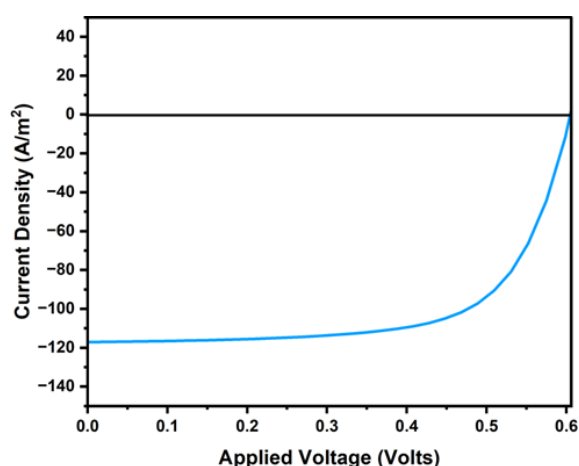| V_{oc} (V)	J_{sc} (A/m^2)	FF	PCE (%)
0.604	-117.35	0.672	4.765

9

Fig. 14. J-V Curve of the organic solar cell

To achieve this, the thicknesses of the hole transport layer, optically active layer, and front and back contacts were optimized to achieve the highest possible power conversion efficiency (PCE) for the solar cell. Following the optimization of other layers, the thickness of the ZnO layer was systematically varied from 0 nm to 60 nm, with intervals of 5 nm.

This range allowed for a comprehensive study of the impact of the ZnO layer thickness on the performance of the solar cell. The variation of Power Conversion Efficiency with the Thickness of the Electron transport layer for the simulated Organic solar cell is represented by Fig. 15. As the ETL thickness increases up to 20nm, the PCE is also observed to be increasing. Then it shows a sudden decrease up to 35 nm thickness of ETL. Thereafter PCE shows a general tendency to increase up an ETL thickness value of 50 nm, by recording its maximum value of 5.384% at 50 nm.

As the ETL thickness is further increased the PCE values are observed to be decreasing, showing the optimized ETL thickness is at 50 nm. The obtained data of Organic Solar cell parameters variation with the thickness of the ZnO layer is presented in Table 5.
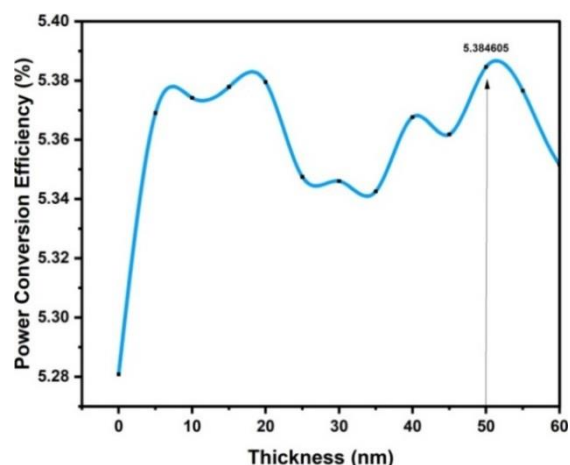

Fig. 15. Variation of Power Conversion Efficiency of Organic solar cell with the Thickness Variation of ETL

3.8. Simulation of Perovskite Cell Using GPVDM

Standard Perovskite $CH_3NH_3PbI_3$ DOS used for solar cell simulation is reported in Table 3. $CH_3NH_3PbI_3$, which is also known as methylammonium lead iodide Perovskite material has revolutionized the field of photovoltaic due to its unique combination of properties. With a Perovskite crystal structure, $CH_3NH_3PbI_3$ stands out due to its cubic lattice framework.

Table 5. The effect of varying the thickness of the ZnO Electron Transport Layer on the performance of the Organic solar cell

Layer thickness (nm)	Active layer	Cathode	Voc (V)	Jsc (A/m^2)	FF	PCE (%)
0	P3HT-PCBM	ZNO/Ag	0.607999	-130.543	0.665337	5.280802
5	P3HT: PCBM	ZNO/Ag	0.608342	-132.294	0.667124	5.369027
10	P3HT: PCBM	ZNO/Ag	0.608342	-132.419	0.667096	5.374150
15	P3HT: PCBM	ZNO/Ag	0.08391	-132.507	0.667095	5.377866
20	P3HT: PCBM	ZNO/Ag	0.608397	-132.536	0.667143	5.379471
25	P3HT: PCBM	ZNO/Ag	0.608204	-131.729	0.667450	5.347474
30	P3HT: PCBM	ZNO/Ag	0.608189	-131.674	0.667564	5.346033
35	P3HT: PCBM	ZNO/Ag	0.608161	-132.165	0.667720	5.342566
40	P3HT: PCBM	ZNO/Ag	0.608328	-132.246	0.667218	5.367675
45	P3HT: PCBM	ZNO/Ag	0.682883	-132.080	0.667435	5.361815
50	P3HT: PCBM	ZNO/Ag	0.608434	-132.6879	0.66675	5.384605
55	P3HT: PCBM	ZNO/Ag	0.608373	-132.4481	0.667250	5.376557
60	P3HT: PCBM	ZNO/Ag	0.608243	-131.8716	0.667206	5.351657

10

The formula $CH_3NH_3PbI_3$ represents the chemical composition of the compound, indicating the presence of methylammonium ($CH_3NH_3^+$) cations, lead (Pb_2^+) cations, and iodide (I^-) anions. This unique structure contributes to a direct band gap, granting the material the ability to effectively capture solar energy. Adding to its capabilities, the material possesses a heightened absorption coefficient, enabling substantial light absorption even in thin layers. This characteristic holds significant importance in the realm of solar cells, where optimizing light absorption remains a pivotal pursuit. Noteworthy attributes like commendable charge carrier mobility, coupled with its compatibility with solution-based processes, further underscore its suitability for seamless integration into solar cell technologies. Simultaneously, researchers are deeply committed to enhancing the stability of perovskite solar cells, to fortify their resilience for practical applications in the real world [71-72]. With optimized values of the active layer and hole transport layer for the experimentally obtained ZnO ETL Layer, simulated Perovskite solar cell structure is shown in Fig.16. The input density of states (DOS) parameters of $CH_3NH_3PbI_3$ (active layer) used for Perovskite solar cell, given in simulator are shown in Table 6 [66]. The same parameters for all layers other than the active layer used in Organic solar cell simulation could be used here in perovskite solar cell simulation. Fig. 17 illustrates the Normalized Photons Absorbed in the simulated Perovskite solar cell.

Here the maximum absorption of photons could be identified between a thickness range of 200-400 nm, which is the active layer region of the Perovskite solar cell. Similar results were available from absorbed photon density simulation which is represented in Fig. 18.

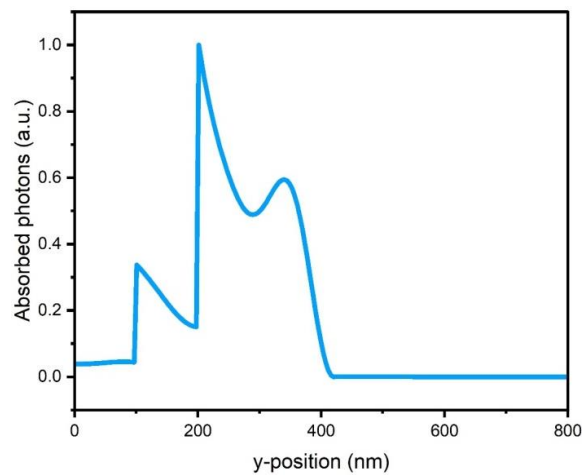**Fig. 16.** Simulated Perovskite Solar cell with layer Thickness

Fig. 17. Normalized Photons Absorbed in the Perovskite solar cell

Table 6. Device parameters: The density of states (DOS) parameters utilized for the Perovskite solar cell simulation

Electron trap density	N_e^{exp}	1×10^{20}	$m^{-3} eV^{-1}$
Hole trap density	N_h^{exp}	1×10^{20}	$m^{-3} eV^{-1}$
Electron tail slope	N_e^U	60×10^{-3}	eV
Hole tail slope	N_h^U	60×10^{-3}	eV
Number of traps		5	
Free electron to trapped electron		1×10^{-20}	m^{-2}
Free hole to trapped hole		1×10^{-20}	m^{-2}
Trapped electron to free hole		1×10^{-22}	m^{-2}
Trapped hole to free electron		1×10^{-26}	m^{-2}
Recombination rate constant	n_{free} to p_{free}	1×10^{-15}	$m^3 s^{-1}$
Electron mobility	μ_{n0}	2×10^{-3}	$m^2 V^{-1} s^{-1}$
Hole mobility	μ_{p0}	2×10^{-3}	$m^2 V^{-1} s^{-1}$
Relative permittivitty	ε_r	20	au
Effective density of free electron states	N_c	1×10^{26}	m^{-3}
Effective density of free hole states	N_v	1×10^{26}	m^{-3}
Affinity	χ_i	3.8	eV
Band gap energy	E_g	1.6	eV

These studies highlight the light-absorbing ability of the simulated Perovskite solar cell. Strategies like adjusting layer thicknesses, exploring different materials, or implementing surface textures to enhance overall light absorption etc can be adopted by photon absorption studies of simulated solar cells, which will ultimately result in improving the solar cell's performance.

Fig. 19 represents the J-V curve of the simulated Perovskite solar cell, showcasing the current-voltage (IV) characteristics of the device under various operating conditions. The fabricated solar cell demonstrated impressive results, with a short-circuit current density (Jsc) of -206.310 A/m² and

an open-circuit voltage (Voc) of 0.623 V. Moreover, it displayed a fill factor (FF) of 0.651 and power conversion efficiency (PCE) of 8.368%. These findings highlight the significant potential of the Perovskite solar cell over Organic solar cells, in efficient energy conversion and performance. The obtained Perovskite solar cell parameters are reported in Table 7.

3.9. Study of Simulated Perovskite Solar Cell Performance by Varying the ETL Thickness

Fig. 20 represents the variation of Power Conversion Efficiency (PCE) with the Thickness of the Electron Transport Layer (ETL) for the simulated Perovskite Solar Cell.
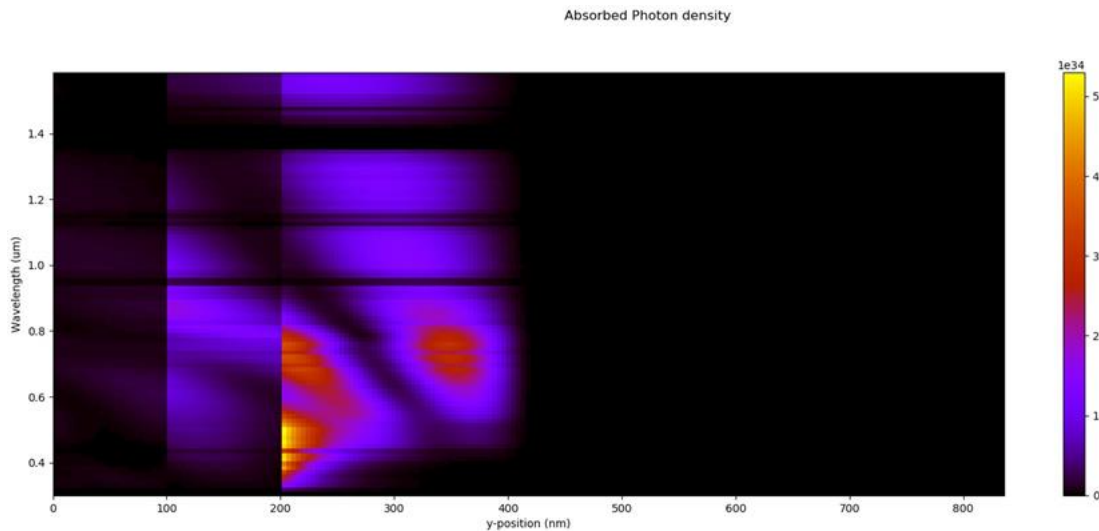

Fig. 18. Absorbed photon density in the Perovskite solar cell

Table 7. Perovskite Solar cell output parameters

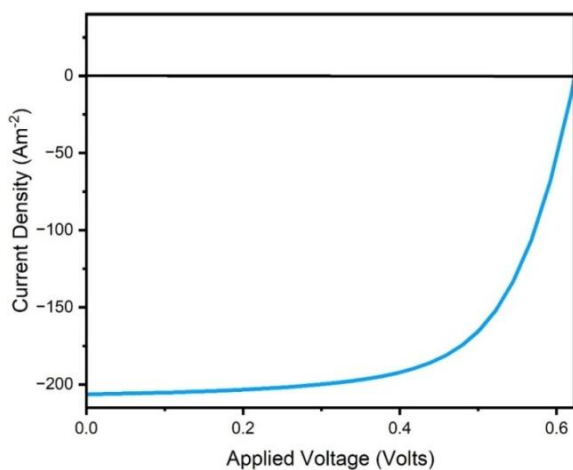| V_{oc} (V)	J_{sc} (A/m²)	FF	PCE (%)
0.623	-206.310	0.651	8.368

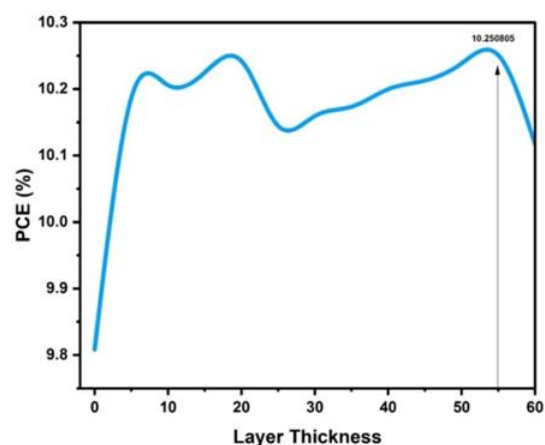**Fig. 19.** J-V Curve of the Perovskite solar cell

Fig. 20. Variation of Power Conversion Efficiency of Perovskite solar cell with the Thickness Variation of ETL

It is observed that as the ETL thickness increases up to 20 nm, the PCE also increases. However, beyond this point, there is a sharp decrease in PCE up to a thickness of 25 nm by recording a minimum value of PCE as 10.114% at 25 nm thickness of ETL.

Further increase of ETL thickness results in the increase of PCE for the device by showing a maximum value of 10.251% at 55 nm of ETL thickness. Further increasing the ETL thickness, results in a decrease in PCE, indicating that the optimized ETL thickness is at 55 nm. The variation of power conversion efficiency of simulated Perovskite solar cells with the increase of 5 nm thickness of ETL is reported in Table 8.

4. CONCLUSIONS

The present study underlines the importance of utilizing SILAR-synthesized zinc oxide thin films as an Electron Transport Layer in organic and perovskite solar cells. The cost-effective SILAR method was used for the deposition of 0.1 Molar ZnO film derived from zinc acetate salt, on a glass substrate. Structural and surface analysis using XRD, SEM, and AFM revealed the crystalline nature, surface texture, and surface roughness of the prepared sample. The film exhibited non-uniform agglomerated grains and stone-like particles distributed on the surface of the substrate. Surface roughness analysis using AFM indicated an R_q to R_a ratio of 1.204. The optical analysis demonstrated the transmittance, absorbance, extinction coefficient, refractive index, and relatively higher Urbach energy with an optical band gap energy of 3.625 eV. Using GPVDM software, the Power Conversion Efficiency of Organic and Perovskite solar cells with a Zinc oxide electron transport layer is determined. The J-V curve analysis using GPVDM revealed the performance of the fabricated solar cells, achieving a notable PCE value of 5.384% and 10.251% respectively for Organic and Perovskite solar cell devices. This study demonstrated that hexagonal wurtzite ZnO thin films deposited by the SILAR method could be used as a potential ETL candidate for solar cell applications. It infers that better efficiency could be achieved by improving the morphological, electrical, and optical properties of the film.

FUNDING

CONFLICT OF INTEREST

The authors declare no conflict of interest.

AUTHOR CONTRIBUTION

All authors (Sreedev P, Rakhesh Vamadevan, Ananthakrishnan A) collaboratively wrote the manuscript, which has been reviewed and approved by each author in its final version.

REFERENCE

[1]. Green, Martin A. "Thin-film solar cells: review of materials, technologies and commercial status." *J. Mat. Sci: Mat in Elec.*, 2007, 18, 15-19.

Table 8. The effect of varying the thickness of the ZnO Electron Transport Layer on the performance of the Perovskite solar cell

Layer thickness (nm)	Active layer	Cathode	Voc (V)	Jsc(A/m^2)	FF	PCE (%)
0	Perovskite	ZNO/Ag	0.628121	-244.342	0.639081	9.808369
5	Perovskite	ZNO/Ag	0.629081	-253.365	0.639141	10.187089
10	Perovskite	ZNO/Ag	0.629141	-254.383	0.639068	10.205762
15	Perovskite	ZNO/Ag	0.629201	-254.305	0.639015	10.224847
20	Perovskite	ZNO/Ag	0.629253	-254.721	0.639002	10.242170
25	Perovskite	ZNO/Ag	0.628929	-252.223	0.639495	10.144348
30	Perovskite	ZNO/Ag	0.28971	-252.557	0.639538	10.159530
35	Perovskite	ZNO/Ag	0.629007	-252.862	0.639616	10.173253
40	Perovskite	ZNO/Ag	0.629114	-253.653	0.6391698	10.199662
45	Perovskite	ZNO/Ag	0.629144	-253.915	0.639294	10.212670
50	Perovskite	ZNO/Ag	0.629249	-254.680	0.638881	10.238527
55	Perovskite	ZNO/Ag	0.6292730	-244.908	0.639051	10.250805
60	Perovskite	ZNO/Ag	0.0628855	-251.602	0.639395	10.116572

[2]. Lee, Taesoo D., and Abasifreke U. Ebong. "A review of thin film solar cell technologies and challenges." *Ren. Sust. Ener.Rev.,* 2017,70, 1286-1297.

[3]. Efaz, Erteza Tawsif, Md Meganur Rhaman, Safayat Al Imam, Khandaker Lubaba Bashar, Fahmid Kabir, MD Ehasan Mourtaza, Syed Nazmus Sakib, and and FA Mozahid. "A review of primary technologies of thin-film solar cells." *Eng. Res. Exp* 3., 2021.3, 032001.

[4]. Marinova, Nevena, Silvia Valero, and Juan Luis Delgado. "Organic and perovskite solar cells: Working principles, materials and interfaces." *J. Coll. Inte. Sci.,* 2017, 488, 373-389.

[5]. Kim, Taewan, Jongchul Lim, and Seulki Song. "Recent progress and challenges of electron transport layers in organic–inorganic perovskite solar cells." *Ene.*13., 2020, 21, 5572.

[6]. Barbé, Jérémy, Max L. Tietze, Marios Neophytou, Banavoth Murali, Erkki Alarousu, Abdulrahman El Labban, Mutalifu Abulikemu et al. "Amorphous tin oxide as a low-temperature-processed electron-transport layer for organic and hybrid perovskite solar cells." *ACS. App. Mat. Inte* 9., 2017, 13, 11828-11836.

[7]. Ghosekar, Ishan C., and Ganesh C. Patil. "Review on performance analysis of P3HT: PCBM-based bulk heterojunction organic solar cells." *Semi. Scie. Tech* 36., 2021, 4, 045005.

[8]. Kadem, Burak, Aseel Hassan, and Wayne Cranton. "Efficient P3HT: PCBM bulk heterojunction organic solar cells; effect of post deposition thermal treatment." *J.Mat. Sci: Mat in Elec,* .2016, 27, 7038-7048.

[9]. Berger, P. R., and M. Kim. "Polymer solar cells: P3HT: PCBM and beyond." *J. Ren. Sust. Ener* 10, 2018, 1.

[10]. Tournebize, Aurélien, Agnès Rivaton, Heiko Peisert, and Thomas Chassé. "The crucial role of confined residual additives on the photostability of P3HT: PCBM active layers.", *J. Phy. Che C* 119., 2015, 17, 9142-9148.

[11]. Bolbol, Ahmed M., Hassan Elshimy, Omar H. Abd-Elkader, M. Kamel, Salah A. Shata, Ahmed M. Tolba, Magdy Ibrahim, and Nasser Y. Mostafa. "Structure and optical properties of Sb-doped $CH_3NH_3PbI_3$: effect on perovskite solar cell performance." *J. Mat. Sci: Mat Elec* 34., 2023. 19, 1489.

[12]. Rajamanickam, Nagalingam, Sudesh Kumari, Venkat Kalyan Vendra, Brandon W. Lavery, Joshua Spurgeon, Thad Druffel, and Mahendra K. Sunkara. "Stable and durable $CH_3NH_3PbI_3$ perovskite solar cells at ambient conditions." *Nanotech.*27., 2016, 23, 235404.

[13]. Mangrulkar, Mayuribala, and Keith J. Stevenson. "The progress of additive engineering for $CH_3NH_3PbI_3$ photo-active layer in the context of perovskite solar cells." *Crys.* 11., 2021, 7, 814.

[14]. Zhang, Shaoqing, Long Ye, Hao Zhang, and Jianhui Hou. "Green-solvent-processable organic solar cells." *Mat. Tod.* 19., 2016, 9, 533-543.

[15]. Zheng, Zhong, Omar M. Awartani, Bhoj Gautam, Delong Liu, Yunpeng Qin, Wanning Li, Alexander Bataller, Kenan Gundogdu, Harald Ade, and Jianhui Hou. "Efficient charge transfer and fine-tuned energy level alignment in a THF-processed fullerene-free organic solar cell with 11.3% efficiency." *Adv. Mat* 29., 2017, 5, 1604241.

[16]. Deng, Kaimo, Qinghua Chen, and Liang Li. "Modification engineering in SnO_2 electron transport layer toward perovskite solar cells: Efficiency and stability." *Adv. Func. Mat* 30., 2020, 46, 2004209.

[17]. Park, Minwoo, Hae Jin Kim, Inyoung Jeong, Jinwoo Lee, Hyungsuk Lee, Hae Jung Son, Dae-Eun Kim, and Min Jae Ko. "Mechanically recoverable and highly efficient perovskite solar cells: investigation of intrinsic flexibility of organic–inorganic perovskite." *Adv. Ene. Mat* 5, 2015, 22, 1501406.

[18]. Yang, Shida, Weifei Fu, Zhongqiang Zhang, Hongzheng Chen, and Chang-Zhi Li. "Recent advances in perovskite solar cells: efficiency, stability and lead-free perovskite." *J. Mat. Chem. A* 5., 2017, 23, 11462-11482.

[19]. Jiang, Qi, Zema Chu, Pengyang Wang, Xiaolei Yang, Heng Liu, Ye Wang, Zhigang Yin, Jinliang Wu, Xingwang Zhang, and Jingbi You. "Planar-structure

perovskite solar cells with efficiency beyond 21%." *Adv. Mat.* 29., 2017.46. 1703852.

[20]. Kim, Jin Young, Jin-Wook Lee, Hyun Suk Jung, Hyunjung Shin, and Nam-Gyu Park. "High-efficiency perovskite solar cells." *Chem.rev.* 120., 2020, 15, 7867-7918.

[21]. Yang, Guang, Hong Tao, Pingli Qin, Weijun Ke, and Guojia Fang. "Recent progress in electron transport layers for efficient perovskite solar cells." *J. Mat. Chem A* 4., 2016, 11, 3970-3990.

[22]. Pramothkumar, A., N. Senthilkumar, Selvakumar Pitchaiya, Nandhakumar Eswaramoorthy, Venkatraman Madurai Ramakrishnan, and I. Vetha Potheher. "Perovskite solar cells: investigation of structural, optical and device performance analysis of Al–Sn co-doped ZnO electron transport layer." *J. Mat. Sci: Mat Elec* 34., 2023, 7 627.

[23]. Sun, Junlu, Nengxu Li, Lin Dong, Xiuxiu Niu, Mengqi Zhao, Ziqi Xu, Huanping Zhou, Chongxin Shan, and Caofeng Pan. "Interfacial-engineering enhanced performance and stability of ZnO nanowire-based perovskite solar cells." *Nanotech* 32., 2021, 47, 475204.

[24]. An, Qingzhi, Paul Fassl, Yvonne J. Hofstetter, David Becker-Koch, Alexandra Bausch, Paul E. Hopkinson, and Yana Vaynzof. "High performance planar perovskite solar cells by ZnO electron transport layer engineering." *Nan. Ener.*, 2017, 39, 400-408.

[25]. Eswaramoorthy, Nandhakumar, and R. Kamatchi. "Planar perovskite solar cells: eco-friendly synthesized cone-like ZnO nanostructure for efficient interfacial electron transport layer." *J. Mat. Sci: Mat. Elec* 32., 2021, 19, 24138-24151.

[26]. Saidani, T., M. Zaabat, M. S. Aida, R. Barille, M. Rasheed, and Y. Almohamed. "Influence of precursor source on sol–gel deposited ZnO thin films properties." *J. Mat. Sci: Mat. Elec.,* 2017, 28, 9252-9257.

[27]. Krishnan, Divya, P. Sreedev, V. Rakhesh, N. S. Roshima, Balakrishnan Shankar, and S. Malavika Sunil. "Comparative optical study of ZnO thin films prepared by SILAR method." In *AIP Conf. Proce*.,. AIP Pub, 2019, 2162.

[28]. Laurenti, Marco, and Valentina Cauda. "Porous zinc oxide thin films: Synthesis approaches and applications." *Coat* 8., 2018, 2, 67.

[29]. Das, Debajyoti, and Praloy Mondal. "Photoluminescence phenomena prevailing in c-axis oriented intrinsic ZnO thin films prepared by RF magnetron sputtering." *Rsc Adv* 4., 2014, 67, 35735-35743.

[30]. Chung, Sung Yun, Sunyoung Kim, Ju-Hyuck Lee, Kyongjun Kim, Sang-Woo Kim, Chong-Yun Kang, Seok-Jin Yoon, and Youn Sang Kim. "All-solution-processed flexible thin film piezoelectric nanogenerator." *Adv. Mat. (Deerfield Beach, Fla.)* 24., 2012, 45, 6022-6027.

[31]. Caglar, Mujdat, Saliha Ilican, Yasemin Caglar, and Fahrettin Yakuphanoglu. "The effects of Al doping on the optical constants of ZnO thin films prepared by spray pyrolysis method." *J. Mat Sci: Mat Elec.*, 2008, 19, 704-708.

[32]. Sreedev, P., Gouri Sreekumar, Aysha A. Samad, V. Rakhesh, and N. S. Roshima. "AFM and UV-visible investigations of ZnO thin film prepared by SILAR method." In *AIP Conf. Proce*, AIP Pub., 2021, 2369.

[33]. Yergaliuly, Gani, Baktiyar Soltabayev, Sandugash Kalybekkyzy, Zhumabay Bakenov, and Almagul Mentbayeva. "Effect of thickness and reaction media on properties of ZnO thin films by SILAR." *Sci rep* 12., 2022, 1, 851.

[34]. Jambure, S. B., S. J. Patil, A. R. Deshpande, and C. D. Lokhande. "A comparative study of physico-chemical properties of CBD and SILAR grown ZnO thin films." *Mat. Res. Bul.,* 2014, 49, 420-425.

[35]. Kaur, Manmeet, M. Shaheera, Ankita Pathak, S. C. Gadkari, and A. K. Debnath. "Highly sensitive NO_2 sensor based on ZnO nanostructured thin film prepared by SILAR technique." *Sens. Actu B: Chem* 2021., 335, 129678.

[36]. Shei, Shih-Chang, Shoou-Jinn Chang, and Pay-Yu Lee. "Rinsing effects on successive ionic layer adsorption and reaction method for deposition of ZnO thin films." *J. Electrochm. Soci* 158., 2010, 3, H208.

[37]. Hima, A., A. Khechekhouche, I. Kemerchou, N. Lakhdar, B. Benhaoua, F. Rogti, I. Telli, and A. Saadoun. "GPVDM simulation of layer thickness effect on power conversion efficiency of CH₃NH₃PbI₃ based planar heterojunction solar cell." *Int. J. Ener* 3., 2018, 1, 37-41.

[38]. Gupta, Vishal, Anju Srivastava, Reena Jain, Vijay Kumar Sharma, and Lalit Kumar. "Optimization and development of ITO-free plasmonic gold nanoparticles assisted inverted organic solar cells." *Opt. Mat.,* 2022. 131, 112747.

[39]. Sims, Lothar, Ulrich Hörmann, Robert Hanfland, Roderick CI MacKenzie, F. René Kogler, Roland Steim, Wolfgang Brütting, and Pavel Schilinsky. "Investigation of the s-shape caused by the hole selective layer in bulk heterojunction solar cells." *Org. Elec* 15., 2014, 11, 2862-2867.

[40]. Puspita, Dita, Ratna Dewi Syarifah, and Nanang Syaiful Rizal. "GPVDM simulation of thickness effect on power conversion efficiency of PEDOT: PSS/P3HT: PCBM solar cell performance." In *AIP Conf. Proce.*, AIP Pub., 2022, 2663.

[41]. Mishra, Amrit Kumar, and R. K. Shukla, "Electrical and optical simulation of typical perovskite solar cell by GPVDM software.", *Mat. Tod. Proc* 49., 2022, 3181-3186.

[42]. Rayner-Canham, Geoff, and Tina Overton, *Des. Inor. Che.*, 2003.

[43]. Devi, P. Geetha, and A. Sakthi Velu, "Synthesis, structural and optical properties of pure ZnO and Co doped ZnO nanoparticles prepared by the co-precipitation method.", *J. Theo. Appl. Phy* 10., 2016, 3, 233-240.

[44]. Wu, Fei, Mengyun Ling, Lingyun Wan, Pei Liu, Yabin Wang, Qiuyu Zhang, and Baoliang Zhang, "Three-dimensional FeMZn (M= Co or Ni) MOFs: Ions coordinated self-assembling processes and boosting microwave absorption.", *Che. Eng. J.*, 2022, 435, 134905.

[45]. Shinde, V. R., T. P. Gujar, C. D. Lokhande, R. S. Mane, and Sung-Hwan Han, "Mn doped and undoped ZnO films: A comparative structural, optical and

electrical properties study.", *Mat. Che. Phy* 2-3., 2006, 96, 326-330.

[46]. Hammad, Talaat M., Jamil K. Salem, and Roger G. Harrison, "Structure, optical properties and synthesis of Co-doped ZnO superstructures.", *App. Nan.*, 2013, 3, 133-139.

[47]. Klug, Harold P., and Leroy E. Alexander, "X-ray diffraction procedures for polycrystalline and amorphous materials.", 1955, 228-235.

[48]. Ahmad, A. A., A. B. Migdadi, A. M. Alsaad, Qais M. Al-Bataineh, and Ahmad Telfah, "Optical, structural, and morphological characterizations of synthesized (Cd–Ni) co-doped ZnO thin films.", *App. Phy. A 12.,* 2021, 127, 922.

[49]. Pehlivanoglu, Seval Aksoy, and Ozgur Polat, "Exploring the structural and optical properties of Ir-doped ZnO thin films.", *Opt. Mat.,* 2023, 143, 114179.

[50]. Teh, Yen Chin, Ala'eddin A. Saif, Z. A. Z. Jamal, and Prabakaran Poopalan, "Microstructure study on Gd-doped BaTiO₃ sol-gel multilayer thin films using AFM for optoelectronic applications.", *Adv. Mat. Res.,* 2014, 911, 251-255.

[51]. Paul, E., J. Temple Black, and A. Kohser Ronald, *MAT. PROC. MANU.*, 2003.

[52]. Nu, S., Au Găsit Rezultate, and Acasă Scoli Teme, "AFM studies on surface morphology, topography and texture of nanostructured zinc aluminum oxide thin films.", 2012.

[53]. Xue, S. W., X. T. Zu, W. L. Zhou, H. X. Deng, X. Xiang, L. Zhang, and H. Deng, "Effects of post-thermal annealing on the optical constants of ZnO thin film.", *J. allo. Comp* 448., 2008, 1-2, 21-26.

[54]. Robert, R., C. Justin Raj, S. Krishnan, and S. Jerome Das, "Growth, theoretical and optical studies on potassium dihydrogen phosphate (KDP) single crystals by modified Sankaranarayanan–Ramasamy (mSR) method.", *Phy. B: Cond. Matt 405.*, 2010, 1, 20-24.

[55]. Alsaad, A. M., Qais M. Al-Bataineh, A. A. Ahmad, Zaid Albataineh, and Ahmad Telfah, "Optical band gap and refractive index dispersion parameters of boron-doped ZnO thin films: A novel derived mathematical model from the experimental

transmission spectra.", *Opt.,* 2020, 211, 164641.

[56]. Tüzemen, Ebru Şenadım, Sıtkı Eker, Hamide Kavak, and Ramazan Esen, "Dependence of film thickness on the structural and optical properties of ZnO thin films.", *App. Surf. Sci 255.,* 2009, 12, 6195-6200.

[57]. Rao, T. Prasada, MC Santhosh Kumar, S. Anbumozhi Angayarkanni, and M. Ashok, "Effect of stress on optical band gap of ZnO thin films with substrate temperature by spray pyrolysis.", *J. Allo. Comp* 485„ 2009, 1-2, 413-417.

[58]. Vimalkumar, T. V., N. Poornima, C. Sudha Kartha, and K. P. Vijayakumar, "Effect of precursor medium on structural, electrical and optical properties of sprayed polycrystalline ZnO thin films.", *Mat. Sci. Eng: B 1.,* 2010, 175, 29-35.

[59]. Hafdallah, A., F. Ynineb, M. S. Aida, and N. Attaf, "In doped ZnO thin films.", *J. Allo. Comp 509.,* 2011, 26, 7267-7270.

[60]. Schönau, S., F. Ruske, S. Neubert, and B. Rech, "Analysis of Urbach-like absorption tails in thermally treated ZnO: Al thin films.", *App. Phy. Lett.,* 2013, 103, 19.

[61]. Ravidas, Babban Kumar, Mukesh Kumar Roy, and Dip Prakash Samajdar, "Investigation of photovoltaic performance of lead-free CsSnI$_3$-based perovskite solar cell with different hole transport layers: First Principle Calculations and SCAPS-1D Analysis.", *Sol. Ene.,* 2023, 249, 163-173.

[62]. Piñón Reyes, Ana C., Roberto C. Ambrosio Lázaro, Karim Monfil Leyva, José A. Luna López, Javier Flores Méndez, Aurelio H. Heredia Jiménez, Ana L. Muñoz Zurita, Francisco Severiano Carrillo, and Esteban Ojeda Durán, "Study of a lead-free perovskite solar cell using CZTS as HTL to achieve a 20% PCE by SCAPS-1D simulation.", *Micr 12.,* 2021, 12, 1508.

[63]. Li, Yongfang, "Molecular design of photovoltaic materials for polymer solar cells: toward suitable electronic energy levels and broad absorption.", *Acc. chem. Res 45.,* 2012, 5, 723-733.

[64]. Shi, Hui, Congcong Liu, Qinglin Jiang, and Jingkun Xu, "Effective approaches to improve the electrical conductivity of PEDOT: PSS: a review.", *Adv. Elec. Mat 1.,* 2014, 4, 1500017.

[65]. Lloyd, Matthew T., Dana C. Olson, Ping Lu, Erica Fang, Diana L. Moore, Matthew S. White, Matthew O. Reese, David S. Ginley, and Julia WP Hsu, "Impact of contact evolution on the shelf life of organic solar cells.", *J. Mat. Chem 19.,* 2009, 41, 7638-7642.

[66]. Puspita, Dita, "Optimation of Layers Thickness Design of Perovskite Solar Cell (PSC) Using GPVDM Simulation.", *Comp. Exp. Res. Mat. Ren. Ener 2.,* 2019, 2, 56-63.

[67]. MacKenzie, Roderick CI, Christopher G. Shuttle, Michael L. Chabinyc, and Jenny Nelson, "Extracting microscopic device parameters from transient photocurrent measurements of P3HT: PCBM solar cells.", *Adv. Ener. Mat 2.,* 2012, 6, 662-669.

[68]. Abdallaoui, M., N. Sengouga, A. Chala, A. F. Meftah, and A. M. Meftah. "Comparative study of conventional and inverted P3HT: PCBM organic solar cell." *Opt Mat* 2020, 105, 109916.

[69]. Wang, Wei, Shaomin Wu, Kitt Reinhardt, Yalin Lu, and Shaochen Chen, "Broadband light absorption enhancement in thin-film silicon solar cells.", *Nan. Lett 10.,* 2010, 6, 2012-2018.

[70]. Proctor, Christopher M., Martijn Kuik, and Thuc-Quyen Nguyen, "Charge carrier recombination in organic solar cells.", *Prog. Poly. Sci 38.,* 2013, 12,1941-1960.

[71]. Yun, Sining, Xiao Zhou, Jacky Even, and Anders Hagfeldt, "Theoretical treatment of CH$_3$NH$_3$PbI$_3$ perovskite solar cells.", *Ang. Chem. Int. Edi 56.,* 2017, 50, 15806-15817.

[72]. Long, Mingzhu, Tiankai Zhang, Yang Chai, Chun-Fai Ng, Thomas CW Mak, Jianbin Xu, and Keyou Yan, "Nonstoichiometric acid–base reaction as reliable synthetic route to highly stable CH3NH3PbI3 perovskite film.", *Nat. Comm 1.,* 2016, 7, 13503.